Distinguishing benign confounding treatment changes from residual prostate cancer on MRI following laser ablation using feature scoring

G. Litjens[a], H. Huisman[a], R. Elliott[b], N. Shih[c], M. Feldman[c], S. Viswanath[b], J. Fütterer[a], J. Bomers[a] and A. Madabhushi[b]

[a]Radboud University Nijmegen Medical Centre, Nijmegen, The Netherlands;
[b]Case Western Reserve University, Cleveland, USA;
[c]University of Pennsylvania, Philadelphia, USA;

ABSTRACT

Laser interstitial thermotherapy (LITT) is a relatively new focal therapy technique for the ablation of localized prostate cancer. In this study we are for the first time integrating ex-vivo pathology and MRI to assess the imaging characteristics of prostate cancer and benign confounding treatment changes following LITT on 3 Tesla multi-parametric MRI. A better understanding of the imaging characteristics of residual disease and succesfully ablated tissue might lead to improved treatment monitoring and as such patient prognosis. A unique clinical trial, in which patients underwent a prostatectomy after LITT treatment, gave us the availability of ex-vivo histology and pre- and post-LITT MRI. Using this data we (1) investigated the imaging characteristics of treatment effects and residual disease and (2) evaluated treatment induced feature changes in the ablated area relative to the residual disease. Towards this end first a pathologist annotated the ablated area and the residual disease on the ex-vivo histology and then we transferred the annotations to the post-LITT MRI using semi-automatic elastic registration. The pre- and post-LITT MRI were subsequently registered and features extracted to determine differences in feature values between residual disease and successfully ablated tissue to assess treatment response. A scoring metric based on change in median pre- and post-LITT feature values was introduced, which allowed us to identify the most treatment responsive features. Finally, we combined this knowledge in a clustering algorithm. Our results show that (1) image characteristics for treatment effects and residual disease are different as evidenced by our ability to, on a voxel-by-voxel basis, classify tissue as residual disease. Furthermore, (2) change of feature values between pre- and post-LITT MRI can be a quantitative marker for treatment response, where especially T2-weighted texture features and DCE MRI features showed large differences between residual disease and successfully ablated tissue. And finally, (3) a clustering approach to separate treatment effects and residual disease incorporating both (1) and (2) yielded a maximum area under the ROC curve of 0.97 on a voxel basis over 3 studies.

Keywords: Laser ablation therapy, prostate cancer, MRI, treatment response

1. INTRODUCTION

Radical treatment of prostate cancer is known for it's relatively high incidence of side-effects like incontinence and impotence. Furthermore, most prostate cancer is not aggressive and might not warrant radical therapy. This has given research into less radical, localized therapy options a lot of traction. Examples are cryo-ablation, high-intensity focused ultrasound or laser-ablation therapy.[1,2] The specific focal therapeutic strategy considered in this work is laser interstitial thermotherapy (LITT). One of the major advantages enjoyed by LITT is its compatibility with magnetic resonance imaging (MRI), allowing for high resolution in vivo imaging to be used in LITT procedures. Furthermore, from previous studies on LITT for liver lesions, we know that the extent of tissue necrosis post-LITT is visible on MRI.[3] However, there is very little work describing the imaging characteristics of LITT-induced changes in the prostate. Understanding changes in MRI imaging features post-LITT is important for accurate follow-up of the patient because it will allow the clinician to assess whether the ablation was successful and whether there is any residual disease present. If residual disease is present, the area could be re-ablated or a different therapy option could be chosen. Furthermore, qualitative observations of LITT-related changes on

prostate MRI do not specifically address how to differentiate between the appearance of benign LITT-related changes (edema, necrosis) that can mask the presence of residual cancer, post-LITT. This implies a need for co-registration and image analysis methods to quantitatively compare pre- and post-LITT MRI in order to identify voxel-by-voxel changes in MRI parameters that can describe LITT-related changes within the prostate.

In this study we take advantage of a unique clinical trial, ongoing at the Radboud University Nijmegen Medical Centre, were we now for the first time have the availability of post-LITT prostatectomy specimens in addition to the pre- and post-LITT MRI. This data allows us to (1) investigate the imaging characteristics of both treatment related changes and residual disease , (2) evaluate treatment induced feature changes in the ablated area relative to the residual disease.

To investigate (1) we first need to identify treatment effects and residual disease on histology and subsequently establish a voxel correspondence between the post-LITT MRI and the histology. To this end first the histology was annotated by a pathologist, after which we performed a careful semi-automatic elastic registration of the histology to the post-LITT MRI. Finally, the histology annotations were propagated to the post-LITT MRI and computer-extracted features were obtained. Features in multi-parametric prostate MRI can be designed for each individual MR parameter, as each parameter characterizes different behavior of the underlying tissue. Multi-parametric prostate MRI typically consists of T2-weighted, diffusion-weighted and dynamic contrast-enhanced imaging.[4,5] The T2-weighted imaging is mostly used for its high resolution and contrast, allowing detailed visualization of the tissue anatomy. From clinical guidelines we know that the T2-weighted images are especially useful to assess the texture of prostate lesions.[5] Prostate cancer exhibits a so-called 'erased charcoal sign', a smudge-like dark texture on T2-weighted images.[5] Furthermore, we know from the work by Viswanath et al. that ablated areas have different textures compared to regular tissue.[6]

Diffusion weighted imaging is specifically useful for characterizing tissue at a microscopic level, enabling us to assess traits like cell density at a macro level. In diffusion weighted imaging, several images with different b-values are acquired. Increasing b-values mean increased diffusion-weighting. Furthermore, to remove protocol dependency an apparent diffusion coefficient map is calculated, which is a roughly quantitative measure of tissue diffusivity. Prostate cancer has a high cellular density compared to the normal glandular structure of the prostate. This results in a reduced diffusivity in cancerous tissue and thus a high signal in high b-value images and subsequently a low apparent diffusion coefficient values. LITT will cause necrosis and formation of scar tissue and might thus alter diffusivity in the tissue. Furthermore, prostate cancer lesions tend to have a focal appearance on diffusion-weighted imaging, which might change due to therapy.

Finally, dynamic contrast enhanced MRI results in signal over time curves and shows the uptake of contrast agent in tissue. This allows us to measure attributes of the tissue vasculature, like the relative fraction of extra-vascular, extra-cellular space in each voxel and micro-vessel permeability. Prostate cancer lesions tend to have leaky micro-vasculature, which results in fast initial enhancement and wash-out. Additionally, inflammation and tissue death (necrosis/apoptosis) caused by the treatment might cause blood flow and vascular changes in the ablated area.

To extract feature changes for (2) we first need to register the pre- and post-LITT to establish voxel correspondence after which we extracted the features for the pre-LITT MRI. Subsequently, a feature score was calculated to identify features which changed most in treatment area, relative to the residual disease. This will allow us to, on a voxel-by-voxel level discriminate between feature changes in residual disease and successfully ablated tissue. After selection of the most relevant feature changes, we built a fuzzy C-means clusterer to improve residual disease detection.

2. PREVIOUS WORK AND NOVEL CONTRIBUTIONS

Treatment evaluation of therapeutic options for prostate cancer have primarily been examined for radiation treatment in a number of qualitative studies.[7,8] For LITT, a Phase I trial found good correlation between volumes of thermal damage that were visible on MRI and those determined via staining of ex vivo surgical prostatectomy specimens from patients who had previously undergone LITT.[9] Additionally while the ablated volume measured on MRI was marginally overestimated compared to pathology, MR images demonstrated excellent capability in discriminating non-viable necrotic tissue, post-ablation.

However, for imaging changes between pre- and post-LITT MRI, only Viswanath et al. investigated the imaging characteristics of LITT related changes on MRI[6] following treatment for prostate cancer as far as the authors know. While they found changes in imaging markers following LITT and specifically found that there were particular imaging markers that revealed more dramatic changes compared to other markers, all the analysis was limited to the ablation zone. Since no histopathology was available, it was not possible to rigorously evaluate whether the changes in imaging markers were driven by treatment effects or by residual disease. Additionally, the lack of histopathology meant that it was not possible to evaluate whether the residual disease had itself undergone any imaging changes and whether these changes were discernible on MRI.

In this work, several novel contributions are made:

- Availability of histology post-LITT allows us to map the extent of the ablated area and residual disease to the post-LITT MRI and extract features for each of the regions specifically.
- Registration of the pre- and post-LITT MRI in conjunction with the mapping from histology allows us to assess which imaging features change due to therapy in both the residual disease and the ablated zone in a high-resolution, voxel-by-voxel way.
- Assess the effect of incorporating feature change into the detection of residual disease on post-LITT MRI to more accurately discriminate between residual disease and treatment effects.

3. EXPERIMENTAL DESIGN

Data description

Initially, four patients who underwent both pre- and post-LITT multi-parametric MRI were included in this study. After the post-LITT MRI all patients underwent a radical prostatectomy. An experienced pathologist annotated areas of LITT induced changes and residual disease on the prostatectomy slide including the largest ablated area. One patient was subsequently excluded because no residual disease was present. Both the pre- and post-LITT MRIs consisted of T2-weighted imaging, a diffusion-weighted sequence including three b-values (50, 400, 800), a dynamic-contrast enhanced time series (36 time points, 4 seconds temporal resolution) and a proton density-weighted image. The scanner software calculated an apparent diffusion coefficient (ADC) based on the diffusion-weighted imaging. A flowchart detailing the data processing is shown in Figure 1

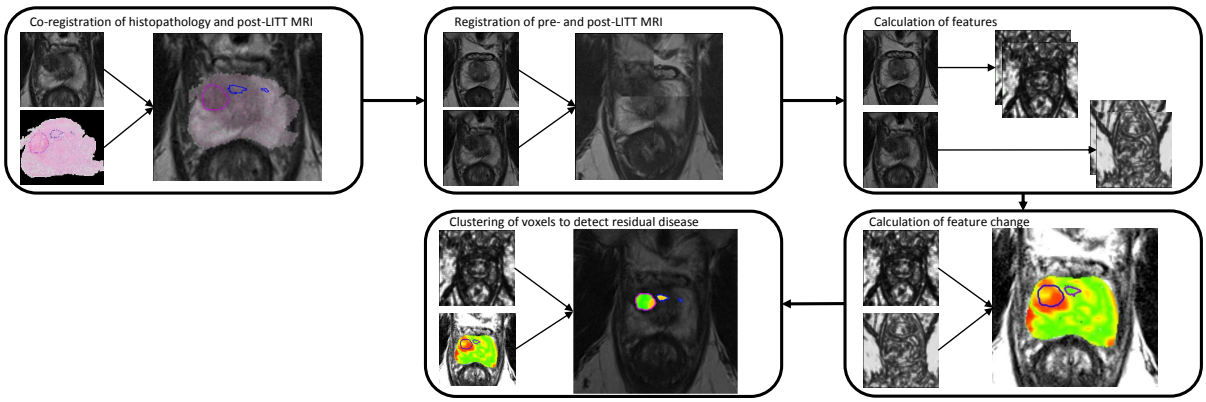

Figure 1. Flowchart detailing the process of co-registration of histopathology and MRI, registration of the pre- and post-LITT MRI, extraction of features and feature change and finally the clustering result to detect residual disease.

Histology/MRI registration

The pathology annotations were transferred to the post-LITT MRI by registering the whole-mount slide to the post-LITT MRI by using a thin plate spline registration technique.[10] The process, in a step-by-step fashion, goes as follows:

1. A pathologist annotates the areas of residual disease and successfully ablated tissue on the whole mount prostatectomy slide using a contouring tool.
2. The slice in the MRI which corresponds to the prostatectomy slide is established by an image analysis researcher under the supervision of a radiologist by comparing landmarks on the pathology and the MRI.
3. Corresponding points are indicated on the prostate boundary for both the prostatectomy slide and the MRI slice.
4. A b-spline transformation is calculated to move from the prostatectomy coordinate space to MRI coordinate space.
5. The histopathology image is transformed to the MRI space using this b-spline transformation and a visual assessment of registration quality is made.
6. The annotations of the pathologist are morphed to the MRI using this b-spline transformation.
7. The pre-LITT MRI is subsequently registered (affine/elastic) to the post-LITT MRI to establish voxel correspondence

An example of the results from this process are show in Figure 2. To establish voxel correspondences between

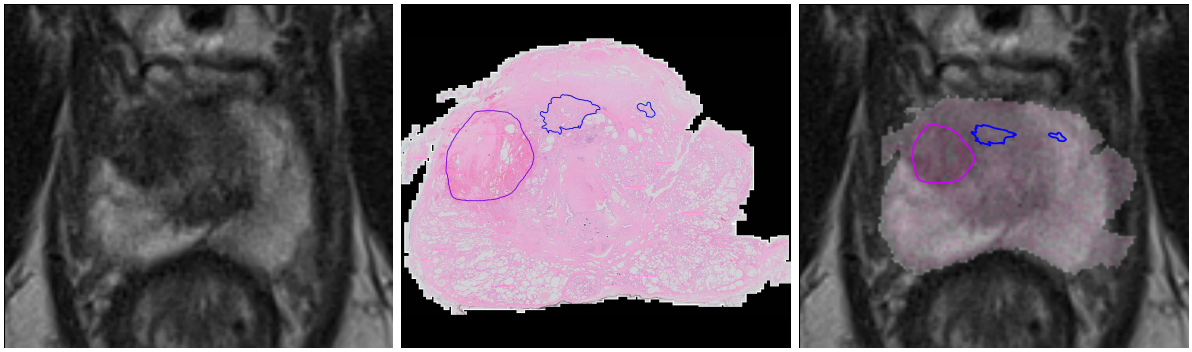

(a) (b) (c)

Figure 2. Example images of the post-LITT MRI (a) and a H&E stained prostatectomy slide (b) and the result of the subsequent MRI/histology registration (c). Ablated area in purple, residual disease in blue

the post- and pre-LITT MRI we used the Elastix registration software.[11] For two out of three patients we applied an affine registration, for one patient we applied an elastic registration because the post-LITT MRI was acquired with an endorectal coil, whereas the pre-LITT MRI was acquired with only a pelvic phased array coil. Registration was performed in two steps, first a translation component was estimated after which either the affine transformation matrix was determined or the b-spline elastic transformation grid. Localized mutual information was used as a similarity metric to drive the registrations.

Feature calculation and scoring

In total 93 features were extracted. An overview of all features used in this study is given in Table 1.

Category	Feature name	Image	Feature settings
Intensity	(Pseudo)T2-map[12]	T2W	
	ADC	DWI	
	b-800	DWI	
Texture	2D Multi-scale Gaussian Derivatives[12]	T2Map	Up to 2nd order, σ=2.0, 2.67, 4.1 and 6.0 mm
	2D Haralick texture measures[10]	T2Map	Kernel sizes 3, 5, 7 voxels
	2D Multi-angle Gabor[10]	T2Map	Four angles: 0, $\frac{\pi}{4}$, $\frac{\pi}{2}$, $\frac{3\pi}{4}$, λ=1.5, 2 and 4 voxels
	2D Li Multi-scale blobness[13]	T2Map, ADC, b800, Ktrans, Kep, Ve, time-to-peak, maximum enhancement, wash-out rate	σ= 2.0, 2.67, 4.1 and 6
Pharmacokinetic	Curve fitting parameters[14]	DCE	Time-to-peak, maximum enhancement, wash-out rate
	Std. Tofts PK model[14]	DCE	Ktrans, Kep, Ve

Table 1. Summary of features and feature settings calculated for both the pre- and post-LITT MRI

Rank	Feature	Median normalized relative change in Residual disease	Treated area
1	Kep	0.05	-0.11
2	Gabor θ=0, λ=1.5	0.07	0.14
3	Gauss. Deriv. - σ=2.0	0.08	0.17
4	T2Map	0.07	0.12
5	Ktrans	0.09	0.15
6	Gauss. Deriv. - σ=2.8	0.09	0.14
7	Haralick Correlation (ws=7)	0.26	-0.40
8	Gabor θ=0.39, λ=1.5	0.09	0.14
9	Gauss. Deriv. X σ=6.0	0.37	0.54
10	Time-to-peak	-0.05	0.07

Table 2. The 10 top scoring features. Columns 3 and 4 show the normalized relative changes (Eq. 1.) in feature value between the pre- and post-LITT MRIs for both residual disease and treated area.

Intensity standardization

Intensity drift is an issue that is well known in MRI.[10] This means that intensities differ from scanner to scanner and even from protocol to protocol on the same scanner. To circumvent this issue in T2-weighted images we can calculate a (pseudo)T2-map using the transverse T2W-image and the proton density-weighted image as described in.[15] This approach uses MR signal equations and a muscle reference region of interest to reduce intensity drift between the pre- and post-LITT acquisition.

T2-weighted imaging features

For the T2-weighted image, we calculated several texture features. We used 13 Haralick texture features using 3 kernel sizes (3,5 and 7 voxels), Gabor texture features using 4 different angles and 3 different wavelengths between 1mm and 6mm and Gaussian derivatives up to second order using 4 different scales between 1mm and 6mm.[10] The texture features were all calculated on the (pseudo)T2-map.

Diffusion-weighted imaging features

For the diffusion-weighted imaging we directly used the ADC values and the b800 image intensities. To take advantage of the fact that prostate lesions tend to exhibit a focal appearance on diffusion-weighted imaging and that treatment effects may not show this feature we implemented the multi-scale blobness filter proposed by Li et al.[16] and calculated the filter using 4 scales between 1 and 6 mm on the b800 and ADC images.

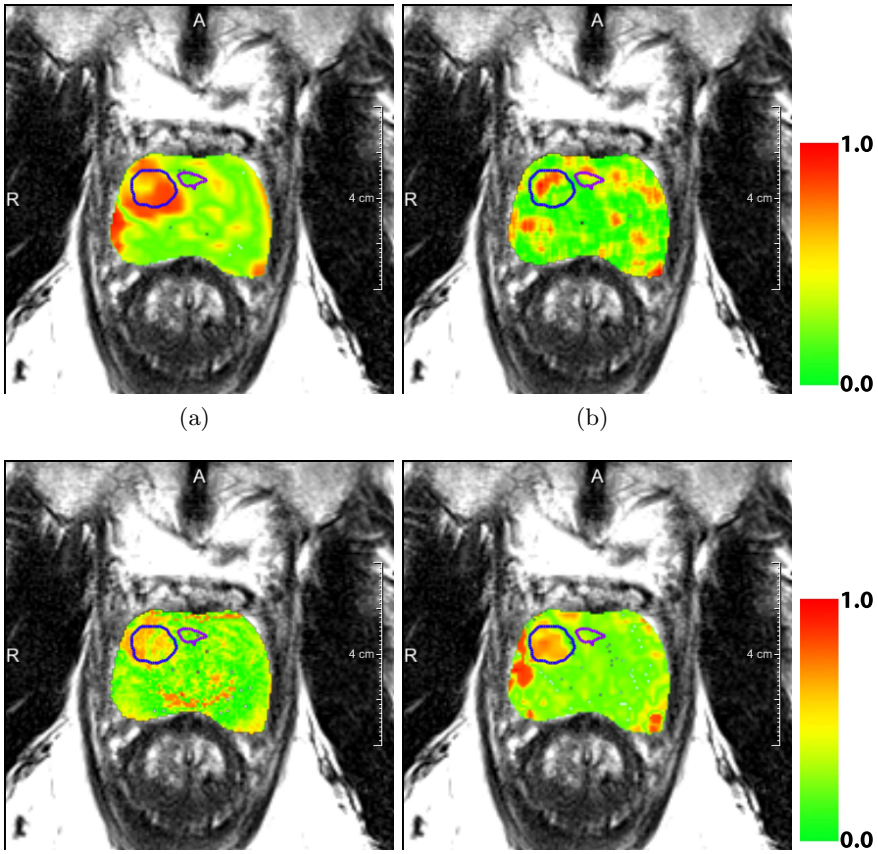

Figure 3. Overlays of normalized feature change between pre- and post treatment MRI. Figures a, b, c and d represent the features Kep, Haralick Correlation, (Pseudo)T2-Map and Ve respectively. The successfully ablated area is indicated in a blue contour and the purple contour indicates residual disease

Dynamic contrast-enhanced imaging features

Dynamic contrast-enhanced MRI also tends to suffer from scanner and protocol dependency. To remove this dependency and extract the most useful information from these curves we implemented curve fitting and pharmacokinetic modeling routines as presented in.[14,17,18] The temporal resolution of the DCE time series was 4 seconds. To capture characteristics on the micro-vasculature we included total of 3 curve features (time-to-peak, washout rate and maximum enhancement)[18] and 3 pharmacokinetic features (Ktrans, Kep, Ve).[14] Furthermore, as cancer also tends to have a focal appearance on DCE MRI we also calculate the Li blobness filter on the Ktrans, Kep, Ve, maximum enhancement, time-to-peak and wash-out rate images.

Feature scoring

The most important diagnostic question after LITT therapy is whether any residual disease is present. To address this question it is important to discriminate between successfully ablated tissue and residual disease. One could only use the information of the post-LITT MRI to answer this question, however, we hypothesize that extra information can be extracted by incorporating change in feature values by using both the pre- and post-LITT MRI. Feature values may change both in the successfully ablated area and in the residual disease area. As such, feature which show a large change in one area and little in the other are most discriminative. We try to quantify this using a feature score. For each feature a score was established by calculating voxel differences between the pre- and post-LITT MRI in both the ablated and residual disease regions. A relative change per feature was

calculated using:

$$d_r(f) = \text{median}_{x \in V} \left(\frac{f_{\text{post}}(x) - f_{\text{pre}}(x)}{f_{\text{pre}}(x)} \right) \quad (1)$$

$$S(f) = ||d_r(f)|_{\text{Res}} - |d_r(f)|_{\text{Abl}}| \quad (2)$$

were d_r is the relative change for feature f. V is the set of all voxels in a region and x is a voxel. f_{post} and f_{pre} are feature f on the post- and pre-LITT MRIs respectively. The score in equation 2 is then defined as the absolute difference between the relative change in the ablated area $d_p(f)_{\text{Abl}}$ and in the residual disease $d_p(f)_{\text{Res}}$. This definition allows us to find features that are important in differentiating between residual disease and therapy effects. The median score over all patients was obtained as the overall score for that feature. Examples of features change is shown in Figure 3

Clustering

A fuzzy C-means clustering to separate residual disease and treatment effects was performed for each patient. The input is unlabeled voxel feature data from the region encompassing both the ablated area and the residual disease. We repeat the clustering 100 times with different initial cluster means to obtain the result with minimal root mean squared error. We perform the experiment with just the calculated features and by adding the change of the top 10 scoring features between the pre- and post-LITT MRI as extra features. This will allow us to asses whether specifically looking at feature change will help to better separate residual disease and treatment effects.

4. EXPERIMENTAL RESULTS AND DISCUSSION

Our objectives were to identify features which (1) allow discrimination between residual disease and treatment effects and (2) showed the most treatment related change relative to residual disease. Finally, we wanted to incorporate this information to (3) improve detection of residual disease. Table 3, column 1 shows that our computer-extracted features are able to identify residual disease with an area under the ROC curve (AUC) up to 0.80 (1). These results also show that extra information, like change of feature values, is needed to obtain higher accuracy in discriminating residual disease from successfully ablated tissue. Furthermore, in Table 2 we present the 10 features with the highest feature change between pre- and post-LITT MRIs (2). One can appreciate that especially the dynamic contrast-enhanced MRI (positions 1, 5, and 10 in Table 2) and the T2-weighted texture features (positions 2, 3, 4, 6, 7, 8, and 9 in Table 2) show large differences between pre- and post-LITT MRI. We hypothesize that due to scar tissue formation in the ablated area the texture changes substantially because most of the scar tissue will be connective tissue, with few live cells. Compared to the residual disease, which will still have a lot of viable cancer cells, it is likely to result in distinct textures.

Furthermore, blood flow and vascular content will be probably be markedly reduced in scar tissue. If we look at Table 2, we can see that the contrast agent transfer constant Kep is markedly reduced in the successfully ablated area, indicating reduced blood low. Furthermore, the time-to-peak has been increased substantially, while it has decreased in the residual disease. The reason time-to-peak reduces in residual disease might be reduced is due to inflammation effects or the cancer needing more nutrients to recover from the effects of the treatment.

As scar tissue also has very limited diffusivity (similar to prostate cancer lesion), the diffusion-weighted imaging might be less useful to assess treatment response, even though it is a very important modality for initial diagnosis of prostate cancer.

Compared to the results of Viswanath et al., we find that diffusion-weighted features seem of less importance. They compared the ablation zone to normal prostate tissue and found diffusion-weighted feature to be most discriminative. In our case, comparing residual disease to successfully ablated tissue, diffusion-weighted features do not seem important. This indicates that, relative to normal tissue, there is a change in diffusion-weighted features, however, that this change is similar in residual disease and successfully ablated tissue. This again shows that diffusion-weighted imaging might be less useful for detection of residual disease.

Finally, combining the computer-extracted features with the relative feature differences, we improved detection of residual disease (3), which is presented quantitatively in Table 3, column 2 and qualitatively in figure

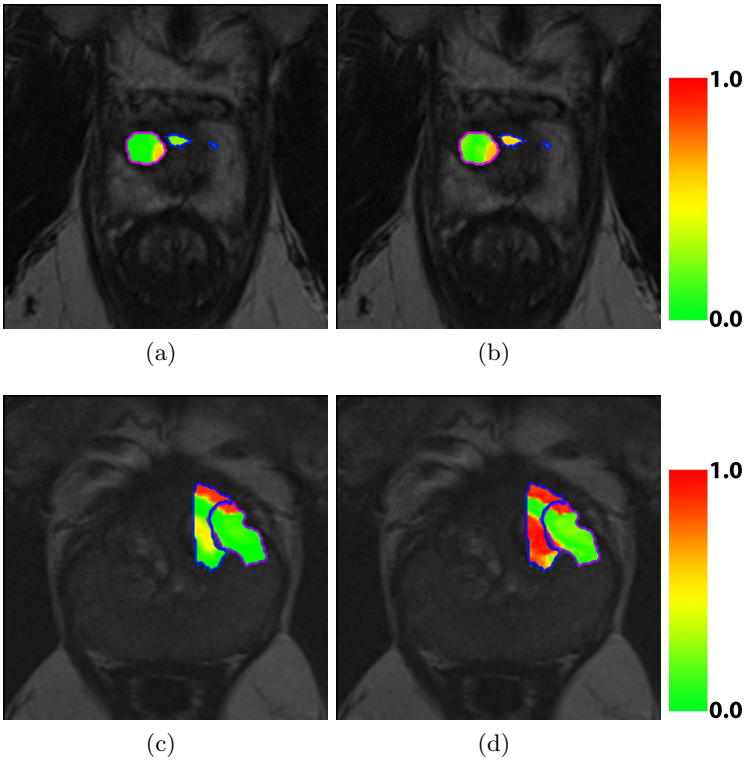

Figure 4. Likelihood heat maps for the fuzzy C-means clustering separating treatment effects and residual disease. Patient 1 (a,b) and patient 3 (c,d) are shown. Figures a,c show the results obtained when only including post-LITT MRI feature, whereas Figures b, d show the improvement obtained by incorporating the 10 highest scoring features (Table 2). Residual disease in blue, ablated area in purple.

4. For all patients we can see that incorporating change in feature values between pre- and post-LITT MRI improves performance substantially. For one patient we were even able to achieve an AUC of 0.97, compared to only 0.80 when using only post-LITT MRI features.

These results shows that, using accurate registration of histopathology and the pre- and post-LITT MRI it is possible to identify features which might be useful in tracking treatment success. Furthermore, in the future we might be able to give quantitative guidelines for the treating physician to help him detect the presence of residual disease and predict patient outcome after successful ablation.

However, our study also has several limitations. The most important one is the lack of additional patient data. Currently, the initial results of the clinical trial are being investigated and will hopefully lead to an extended clinical trial. This will allow us to perform statistical tests to asses the significance of our results. Additionally, this will open up the opportunity to do a supervised classification of residual disease on the post-LITT MRI, which is now limited due to the substantial differences in treatment response in the three patients. Finally, the pathology MRI/co-registration is on a 2D basis whereas a fully 3D pipeline would most likely further improve results.

5. CONCLUDING REMARKS AND CONTRIBUTIONS

In this work we used a unique ongoing clinical trial involving prostate cancer patients being treated with LITT followed by radical prostatectomy to address a unique set of questions: (1) are there imaging characteristics specific for residual disease and treatment effects? (2) Can we identify features which showed the most treatment related change relative to residual disease? And (3) can we improve detection of residual disease by incorporating feature change in addition to post-LITT MRI features? By co-registering histology, pre- and post-LITT MRI we

Patient	Features	Features + feature differences
Patient 1	0.80	0.97
Patient 2	0.62	0.69
Patient 3	0.69	0.78

Table 3. Area under the curve on a voxel-by-voxel basis for detecting residual disease. The second column shows the effect of adding the differences between pre- and post-LITT MRI for the 10 scoring features as extra features (Table 2).

were able to identify features which are able to (1) discriminate between residual disease and treatment effects (AUC up to 0.80, Table 3). However, the results over all three patients showed that more information is needed to increase accuracy in the detection of residual disease, for example by incorporating feature change.

Furthermore, we identified (2) the 10 most relevant features for assessing treatment induces changes (Table 2), which in the future could be used to asses treatment response in longitudinal studies. The most important features that where picked up where T2-weighted texture features and DCE MRI features, whereas diffusion-weighted imaging is usually considered the most important modality in the initial diagnosis of prostate cancer. We hypothesize that the changes in the texture and DCE feature are caused by formation of scar tissue in the successfully ablated area, whereas the residual disease will try to recover from the treatment effects, and as such will try to increase the flow of nutrients.

Finally, we were able to (3) improve detection of residual disease using a per-patient clustering incorporating feature change (AUC for identifying residual disease up to 0.97). This implies that physicians might in the future be able to use these image analysis techniques to assess treatment success and predict the possibility of biochemical recurrence. In future work we intend to evaluate our data on a larger cohort and investigate the use of supervised classification over clustering.

REFERENCES

[1] Rosenkrantz, A. B., Scionti, S. M., Mendrinos, S., and Taneja, S. S., "Role of MRI in minimally invasive focal ablative therapy for prostate cancer," *AJR Am J Roentgenol* **197**, W90–W96 (2011).

[2] Oto, A., Sethi, I., Karczmar, G., McNichols, R., Ivancevic, M. K., Stadler, W. M., Watson, S., and Eggener, S., "MR imaging-guided focal laser ablation for prostate cancer: phase I trial," *Radiology* **267**, 932–940 (2013).

[3] Roberts, H. R., Paley, M., Hall-Craggs, M. A., Lees, W. R., Friedman, E. P., Clemence, M., Buonacorssi, G., and Bown, S. G., "Dynamic magnetic resonance control of interstitial laser photocoagulation therapy of colorectal hepatic metastases," *Lancet* **343**, 1221 (1994).

[4] Kitajima, K., Kaji, Y., Fukabori, Y., Yoshida, K., Suganuma, N., and Sugimura, K., "Prostate cancer detection with 3 T MRI: Comparison of diffusion-weighted imaging and dynamic contrast-enhanced MRI in combination with T2-weighted imaging," *J Magn Reson Imaging* **31**, 625–631 (2010).

[5] Barentsz, J. O., Richenberg, J., Clements, R., Choyke, P., Verma, S., Villeirs, G., Rouviere, O., Logager, V., Fütterer, J. J., and European Society of Urogenital Radiology, "ESUR prostate MR guidelines 2012," *Eur Radiol* **22**, 746–757 (2012).

[6] Viswanath, S., Toth, R., Rusu, M., Sperling, D., Lepor, H., Futterer, J., and Madabhushi, A., "Quantitative evaluation of treatment related changes on multi-parametric MRI after laser interstitial thermal therapy of prostate cancer," in [*Proceedings of the SPIE*], 86711F–86711F, International Society for Optics and Photonics (2013).

[7] Pickett, B., Kurhanewicz, J., Coakley, F., Shinohara, K., Fein, B., and Roach, 3rd, M., "Use of MRI and spectroscopy in evaluation of external beam radiotherapy for prostate cancer," *Int J Radiat Oncol Biol Phys* **60**, 1047–1055 (2004).

[8] Song, I., Kim, C. K., Park, B. K., and Park, W., "Assessment of response to radiotherapy for prostate cancer: value of diffusion-weighted MRI at 3 t," *AJR Am J Roentgenol* **194**, W477–W482 (2010).

[9] Lindner, U., Lawrentschuk, N., Weersink, R. A., Davidson, S. R. H., Raz, O., Hlasny, E., Langer, D. L., Gertner, M. R., Van der Kwast, T., Haider, M. A., and Trachtenberg, J., "Focal laser ablation for prostate cancer followed by radical prostatectomy: validation of focal therapy and imaging accuracy," *Eur Urol* **57**, 1111–1114 (2010).

[10] Viswanath, S. E., Bloch, N. B., Chappelow, J. C., Toth, R., Rofsky, N. M., Genega, E. M., Lenkinski, R. E., and Madabhushi, A., "Central gland and peripheral zone prostate tumors have significantly different quantitative imaging signatures on 3 tesla endorectal, in vivo T2-weighted MR imagery," *J Magn Reson Imaging* **36**, 213–224 (2012).

[11] Klein, S., Staring, M., Murphy, K., Viergever, M. A., and Pluim, J. P. W., "elastix: a toolbox for intensity-based medical image registration," *IEEE Trans Med Imaging* **29**, 196–205 (2010).

[12] Litjens, G. J. S., Debats, O. A., van de Ven, W. J. M., Karssemeijer, N., and Huisman, H. J., "A pattern recognition approach to zonal segmentation of the prostate on MRI," in [*Med Image Comput Comput Assist Interv*], *Lect Notes Comput Sci* **7511**, 413–420 (2012).

[13] Li, Q., Sone, S., and Doi, K., "Selective enhancement filters for nodules, vessels, and airway walls in two- and three-dimensional CT scans," *Med Phys* **30**, 2040–2051 (2003).

[14] Vos, P. C., Barentsz, J. O., Karssemeijer, N., and Huisman, H. J., "Automatic computer-aided detection of prostate cancer based on multiparametric magnetic resonance image analysis," *Phys Med Biol* **57**, 1527–1542 (2012).

[15] Litjens, G., Barentsz, J., Karssemeijer, N., and Huisman, H., "Automated computer-aided detection of prostate cancer in MR images: from a whole-organ to a zone-based approach," in [*Medical Imaging*], *Proceedings of the SPIE* **8315**, 83150G–83150G–6 (2012).

[16] Li, B., Christensen, G. E., Hoffman, E. A., McLennan, G., and Reinhardt, J. M., "Establishing a normative atlas of the human lung: Intersubject warping and registration of volumetric CT images," *Acad Radiol* **10**, 255–265 (2003).

[17] Tofts, P. S., Brix, G., Buckley, D. L., Evelhoch, J. L., Henderson, E., Knopp, M. V., Larsson, H. B., Lee, T. Y., Mayr, N. A., Parker, G. J., Port, R. E., Taylor, J., and Weisskoff, R. M., "Estimating kinetic parameters from dynamic contrast-enhanced t(1)-weighted MRI of a diffusable tracer: standardized quantities and symbols," *J Magn Reson Imaging* **10**, 223–232 (1999).

[18] Huisman, H. J., Engelbrecht, M. R., and Barentsz, J. O., "Accurate estimation of pharmacokinetic contrast-enhanced dynamic MRI parameters of the prostate," *J Magn Reson Imaging* **13**, 607–614 (2001).